Published in final edited form as:
Angew Chem Int Ed Engl. 2013 December 9; 52(50): . doi:10.1002/anie.201306306.

Chelator-Free Synthesis of a Dual-Modality PET/MRI Agent

Dr. Feng Chen
Department of Radiology, University of Wisconsin - Madison, 1111 Highland Avenue, Madison, WI, 53705, Fax: (+1) 608-265-0614

Dr. Paul A. Ellison
Department of Medical Physics, University of Wisconsin – Madison

Christina M. Lewis
Department of Medical Physics, University of Wisconsin – Madison

Dr. Hao Hong
Department of Radiology, University of Wisconsin - Madison, 1111 Highland Avenue, Madison, WI, 53705, Fax: (+1) 608-265-0614

Dr. Yin Zhang
Department of Medical Physics, University of Wisconsin – Madison

Sixiang Shi
Materials Science Program, University of Wisconsin – Madison

Dr. Reinier Hernandez
Department of Medical Physics, University of Wisconsin – Madison

Prof. M. Elizabeth Meyerand
Department of Medical Physics, University of Wisconsin – Madison

Todd E. Barnhart
Department of Medical Physics, University of Wisconsin – Madison

Prof. Weibo Cai*
Department of Radiology, University of Wisconsin - Madison, 1111 Highland Avenue, Madison, WI, 53705, Fax: (+1) 608-265-0614

Materials Science Program, University of Wisconsin – Madison

Keywords

radioarsenic; SPION; PET; MRI; lymph node mapping; multimodality imaging

Most of the radiometals with physical properties suitable for imaging and/or therapy applications (e.g. ^{64}Cu, ^{89}Zr, ^{99m}Tc, ^{111}In, ^{177}Lu, ^{90}Y, etc.) require the coordination of certain chelators to form stable complexes.[1] Due to the uniqueness of each radionuclide, knowing the particular coordination chemistry and selecting the best chelator with sufficient in vivo stability are a vital, however, highly challenging task. Therefore, the development of a stable radiopharmaceutical that contains both diagnostic and therapeutic radioisotopes, labeled via a simple but effective chelator-free strategy, is highly desirable.

[*] WCai@uwhealth.org.
[**]F. Chen and P. A. Ellison contributed equally to this work.

Supporting information for this article is available on the WWW under http://www.angewandte.org or from the author.

Combination of positron emission tomography (PET) and magnetic resonance imaging (MRI) has attracted tremendous interest over the last decade, and commercial PET/MRI scanners have become commercially available.[2] The future of PET/MRI scanners will greatly benefit from the use of dual-modality PET/MRI probes. Many dual-modality PET/MRI agents have been reported, which are typically synthesized by radiolabeling magnetic nanoparticles.[3]

Arsenic (As) has 4 positron emitting ($^{70/71/72/74}$As) and 3 electron emitting ($^{74/76/77}$As) radioisotopes with half-lives ranging from 52.6 min to 17.8 days (Table S1), which could be useful for both PET and internal radiotherapy applications.[1] However, the use of arsenic isotopes has been quite scarce due to limited availability, because of difficulties related to isotope production, separation, and purity of the radionuclides.[4] Furthermore, few techniques are currently available for incorporation of these radionuclides into biologically relevant targeting vectors. To the best of our knowledge, labeling antibodies and polymers through covalent interaction of radioactive arsenite, i.e., *As(III), with sulfhydryl groups is the only reported method,[5] while techniques for labeling of radioactive arsenate, i.e., *As(V), are still unavailable.

Fortunately, the incorporation of both As(III) and As(V) into the magnetite or superparamagnetic iron oxide nanoparticle (SPION) structures has long been observed and is still used for the groundwater decontamination process.[6] In addition, underlying chemical mechanism of such highly specific and efficient arsenic trapping by magnetite has also been elucidated recently.[7] The high affinity of As for the magnetite surface has been suggested to be related to the formation of highly stable As-complexes, where the As(III)O_3 pyramids or As(V)O_4 tetrahedra occupy vacant FeO_4 tetrahedral sites on the octahedrally terminated {111} surface of the magnetite nanoparticles.[7]

Inspired by these results, for the first time, we demonstrate here a simple but highly efficient strategy for the synthesis of radioarsenic-labeled SPION (i.e., *As-SPION, *=71, 72, 74, 76) without the use of any chelators. Our hypothesis is that, by simply mixing water soluble SPION with *As(III) or *As(V) species, a novel dual-modality PET/MRI agent of *As-SPION could be easily formed due to the strong and specific affinity of *As to the surface of SPION (Figure 1a).

Figure 1b shows the transmission electron microscopy (TEM) image of oleic-acid (OA) capped ~10 nm sized SPIONs with irregular morphologies, which were synthesized via a well-established thermal decomposition method.[8] As-synthesized SPIONs were coated with a layer of OA surfactant, which could only be well-dispersed in nonpolar organic solvents (e.g., cyclohexane) and exhibited superparamagnetism at room temperature (Figure 1b-inset). The X-ray diffraction pattern of as-synthesized SPION matches well with standard Fe_3O_4 reflection (JCPDS No. 89-0691), as shown in Figure S1. A well-established ligand-exchange process was used to replace the original OA ligands with poly(acrylic acid) (PAA),[9] which efficiently transferred SPION@OA from the organic phase to the aqueous phase (Figure 1c-inset), resulting in PAA modified SPION (i.e., SPION@PAA). The TEM image in Figure 1c confirmed that there is no obvious change of SPION in either particle size or morphology after ligand exchange. Dynamic light scattering (DLS) of SPION@PAA in PBS (pH 7.4) solution showed a diameter of 23.1 nm (which includes the surface coating and hydration layer), larger than the core size observed from TEM (~10 nm). As-synthesized SPION@PAA was found to be highly stable in many different biological solutions, such as phosphate-buffered saline (PBS), saline, and fetal bovine serum, with no visible aggregation for more than 6 months (Figure S2).

The radioarsenic was produced by irradiating natural germanium oxide targets with protons using the University of Wisconsin GE PETtrace Cyclotron. Irradiated targets were processed in a multistep chemical isolation procedure adapted from literature,[5c, 10] involving dissolution, precipitation, filtration, evaporation, anion exchange chromatography, reduction, and solvent extraction. This four-hour procedure gave a non-decay-corrected radioarsenic yield of 49 ± 12 % (n = 13), resulting in a mixture of *As(III) and *As(V) in a small volume of aqueous solution (pH 4.5) with no detectable radiocontaminants.

The oxidation state of radioarsenic at the end of the separation procedure was initially *As(III) as *$As(OH)_3$, which was observed to rapidly auto-oxidize to *As(V), forming H_3*AsO_4. The rate of this auto-oxidation varied widely over the conducted experiments. As a result, the following *As-labeling to SPION experiments were conducted with a mixture of *As(III) as *$As(OH)_3$ and *As(V) as $[H_2{}^*AsO_4]^{-1}$ and $[H{}^*AsO_4]^{-2}$ in solution with *As(III)/*As(V) ratios ranging from <0.1 to ~0.8. The oxidation state of the radioarsenic could be monitored through the separation and nanoparticle labeling procedures using thin layer chromatography (TLC) visualized by autoradiography.

The pH- and oxidation state-dependent sorption behaviors of arsenic to magnetite have already been well-documented.[6d] Considering the co-existence of *As(III) and *As(V) after the generation of radioarsenic, we fixed the pH to 7-8 in the following studies to optimize the *As-labeling yield. Radiolabeling yields were calculated by spotting analyte on 250 μm SiO_2, styrene backing TLC plates and developed with a 0.01 M sodium tartrate/ methanol (3:1) solution as the mobile phase. The distribution of radioarsenic was visualized by exposing a Packard multisensitive phosphor screen to the developed, dried, tape-covered plates, followed by processing with a Perkin Elmer Cyclone Plus Storage Phosphor System. *As-SPION nanoparticles (R_F = 0) could be well-distinguished from free *As(III) (R_F of ~ 0.8) and *As(V) (R_F of ~ 0.95) using this analytical procedure (Figure S3).

Immediately after the mixing of *As with water soluble SPION@PAA (in 1 mM of sodium hydroxide, pH 7-8), 47.3% of *As was strongly absorbed to the SPION surface (Figure 1d, e). The *As-labeling yield exhibited a sharp increase to 84.2% within 2 h of incubation (specific radioactivity: ~3.0 MBq/μmol of Fe), and slowly reached the maximal labeling yield of 92.2% after 24 h (Figure 1d and Figure S4a). Negative control group (Figure 1d and Figure S4c) without SPION was performed to confirm the successful labeling of *As to SPION.

The competitive adsorption between As and other ions (e.g., phosphate and citrate) to iron oxides has been reported.[11] For example, adsorption of As(III) and As(V) on hydrated iron oxide could be suppressed in the presence of phosphate.[11b] To confirm the specific adsorption of *As to SPION, solvent with competitive ions of sodium citrate (17 mM, pH 7-8) was used to inhibit the adsorption of *As to SPION. Figure 1d (and Figure S4b) clearly showed an about 2-fold reduction of *As-labeling yield after 2 h of incubation (43.7% VS 84.2%) of *As with SPION@PAA and sodium citrate. No significant changes in *As-labeling yield could be found after further increasing the concentration of sodium citrate to 340 mM (Figure S5a). The Fe concentration dependent *As-labeling yield was also demonstrated, where higher concentration of SPION showed expected higher *As-labeling yield (Figure S5b).

We hypothesize that coating of SPION with a dense silica ($dSiO_2$) shell or incubating *As with non-magnetite nanoparticles could prevent the absorption of *As, as they are not expected to form stable *As(III) or *As(V) complexes.[7] To further demonstrate the high specificity of *As labeling to SPION, two control studies were performed. Incubation of the same amount of *As with citrate capped copper sulfide (CuS) nanoparticles or

SPION@dSiO$_2$ showed no obvious labeling of *As (Figure 1e and Figure S6), clearly indicating the high labeling efficiency and specificity of *As to SPION. Taken together, our systematic investigation demonstrated the successful labeling of *As to SPION, which is fast, Fe concentration-dependent, and highly specific.

To demonstrate the capability of *As-SPION for dual-modality PET/MRI, phantom studies were first performed. Figure 2a and 2b shows the PET images of *As-SPION with varied radioactivity (from 0 to 1.50 MBq) and Fe concentrations (from 0 to 15.5 mM). Since no radioactive materials (e.g., *As-SPION) are allowed in our 4.7 T microMRI scanning room, SPION with the same Fe concentrations as in Figure 2b were used to demonstrate the enhanced T_2* MR contrast. Figure 2c clearly shows the decrease of T_2 relaxation time (from 484.4 to 5.4 ms) with the increase of Fe concentrations (from 0 to 1.94 mM), consistent with the corresponding T_2*-weighted MR images. T_2 relaxation time was too short to be measured at Fe concentrations equal to or exceeding 3.88 mM, due to lack of measurable signal (indicated by dashed circles). The T_2 relaxivity (r_2) of SPION@PAA was found to be 93.8 $mM^{-1}s^{-1}$ in the 4.7 T microMRI scanner (Figure S7).

To demonstrate the feasibility of *As-SPION for dual-modality PET/MRI imaging and investigate their biodistribution in vivo, 200 μL of *As-SPION (~5.5 MBq) was intravenously (i.v.) injected into normal BALB/c mice. Strong liver (32.5 ± 0.7, 25.7 ± 1.6, and 16.1 ± 2.5 %ID/g at 0.5, 2.5 and 15 h post-injection [p.i.], respectively, n = 2) and bladder (18.5 ± 3.2, 58.3 ± 5.6, and 5.3 ± 4.9 %ID/g at 0.5, 2.5 and 15 h p.i., respectively) uptake of *As-SPION was observed, as shown in Figure 3b. Since the DLS diameter of *As-SPION is significantly larger than the renal clearance threshold (~5.5 nm),[12] the bladder radioactivity signal is likely due to the desorption of *As from SPION under biological conditions.

We further demonstrated that such desorption of *As could be significantly reduced by coating *As-SPION with a layer of polyethylene glycol (PEG). As shown in Figure 3a, strong liver uptake of *As-SPION@PEG was observed (25.0 ± 2.7, 24.8 ± 3.2, 11.0 ± 1.4 %ID/g at 0.5, 2 and 20 h p.i., respectively, n = 4), with significantly lower bladder signal (12.0 ± 1.3, 11.7 ± 3.2, 3.9 ± 2.2 %ID/g at 0.5, 2 and 20 h p.i., respectively, n = 4) after i.v. injection of mice with *As-SPION@PEG. The enhanced stability of *As-SPION@PEG was also confirmed by incubation in complete mouse serum at 37 °C for 24 h (Figure S8). Efforts in further optimizing the stability of *As-SPION in vivo are needed.

In comparison with the biodistribution patterns of free *As (Figure 3c), which shows fast renal clearance and nearly no liver uptake of *As, the strong radioactivity signal from the liver in Figure 3a and 3b were indeed originated from *As-SPION@PEG (or *As-SPION) but not free *As. The liver uptake of *As-SPION was further confirmed by in vivo MR imaging, which clearly shows darkening of the liver and no detectable signal change in the kidney (or bladder) after i.v. injection of SPION@PAA (Figure 3d). The biodistribution of *As-SPION@PEG was further investigated at 20 h p.i., after euthanizing the mice after the last PET scans and measuring the tissue radioactivity in a γ-counter (Figure S9). Dominant uptake of *As-SPION@PEG in both the liver and spleen was observed, validating that serial PET imaging in Figure 3a truly reflected the distribution pattern of *As-SPION@PEG in mice. Similar uptake of the other PET/MRI contrast agents (e.g. ^{64}Cu-labeled SPION) by liver and spleen has also been reported previously, which is commonly observed for intravenously injected nanoparticles.[3b, 13]

The lymphatic system is an important first line of defense against infection, and it is also a common route for cancer metastasis.[14] Therefore, sentinel lymph node mapping is of critical importance in clinical cancer patient management.[15] We further demonstrated that

*As-SPION@PEG could also be used as a dual-modality PET/MRI probe for lymph node mapping. Upon subcutaneous injection of 40 μL of *As-SPION@PEG (~3 MBq) into the right footpad of normal BALB/c mice, serial PET scans were performed. Clear accumulation of *As-SPION@PEG in the popliteal lymph node could be seen at 2.5 and 15 h p.i. (Figure 4a), with the uptake of *As-SPION@PEG found to be 12.5 and 13.2 %ID/g, respectively (Figure 4b). The accumulation of SPION@PAA in one of the lymph nodes (dashed circle in Figure 4c) could also be clearly visualized by MRI, which shows gradual darkening of the lymph node after injection of SPION@PAA (40 μL, 7.77 mM of Fe) into the footpad of mice. As an internal control, the contralateral lymph node (solid circle in Figure 4c) showed no contrast enhancement.

Although dual-modality PET/MRI imaging could only be achieved separately in our current work due to the lack of an integrated microPET/microMRI scanner, this work serves as an important proof-of-concept to establish *As-SPION as a promising candidate for simultaneous PET/MRI. With further development of scanners integrating whole body MRI with simultaneous acquisition of PET, such as the Siemens Biograph mMR system, imaging agents like *As-SPION will be necessary to take advantage of the high sensitivity of PET and exquisite soft tissue contrast of MRI for future cancer patient management. Since the labeling of radioarsenic is not limited to positron-emitting *As, other radioarsenic isotopes with therapeutic capability (e.g., $^{76/77}$As) could also be readily used for the integration of PET/MRI imaging with internal radiotherapy. With the presence of carboxyl groups at the surface of *As-SPION, further conjugation of specific targeting ligands such as proteins/antibodies/peptides[16] could be readily achieved, which will make this class of agents even more powerful in future cancer-targeted PET/MRI and simultaneous radiotherapy, as well as many other clinical scenarios.

In conclusion, we have developed a novel dual-modality PET/MRI agent *As-SPION by mixing irregularly-shaped SPION with radioarsenic. In comparison with the majority of PET/MRI agents reported to date,[3, 17] our method does not require the use of any chelators and is applicable for labeling radioarsenic in both stable oxidation states. Upon optimization as described above, *As labeling of SPION was demonstrated to be fast, Fe concentration-dependent, and highly specific. The biodistribution pattern and feasibility of our new PET/MRI agent for dual-modality imaging in vivo and lymph node mapping have also been investigated and demonstrated.

Supplementary Material

Refer to Web version on PubMed Central for supplementary material.

Acknowledgments

[***]
This work is supported, in part, by the University of Wisconsin - Madison, the National Institutes of Health (NIBIB/NCI 1R01CA169365, T32CA009206, and T32GM08349), the Department of Defense (W81XWH-11-1-0644), and the American Cancer Society (125246-RSG-13-099-01-CCE). The authors thank Prof. R. J. Nickles and Prof. O. T. DeJesus for helpful discussions related to production and isolation of radioarsenic.

References

1. Cutler CS, Hennkens HM, Sisay N, Huclier-Markai S, Jurisson SS. Chem. Rev. 2013; 113:858–883. [PubMed: 23198879]
2. Balyasnikova S, Lofgren J, de Nijs R, Zamogilnaya Y, Hojgaard L, Fischer BM. Am. J. Nucl. Med. Mol. Imaging. 2012; 2:458–474. [PubMed: 23145362]

3. a) Choi JS, Park JC, Nah H, Woo S, Oh J, Kim KM, Cheon GJ, Chang Y, Yoo J, Cheon J. Angew. Chem. Int. Ed. 2008; 47:6259–6262.b) Lee HY, Li Z, Chen K, Hsu AR, Xu C, Xie J, Sun S, Chen X. J. Nucl. Med. 2008; 49:1371–1379. [PubMed: 18632815]
4. Jennewein M, Qaim SM, Hermanne A, Jahn M, Tsyganov E, Slavine N, Seliounine S, Antich PA, Kulkarni PV, Thorpe PE, Mason RP, Rosch F. Appl. Radiat. Isot. 2005; 63:343–351. [PubMed: 15955705]
5. a) Jennewein M, Hermanne A, Mason RP, Thorpe PE, Rösch F. Nucl. Instrum. Methods Phys. Res. 2006; 569:512–517.b) Jennewein M, Lewis MA, Zhao D, Tsyganov E, Slavine N, He J, Watkins L, Kodibagkar VD, O'Kelly S, Kulkarni P, Antich PP, Hermanne A, Rosch F, Mason RP, Thorpe PE. Clin. Cancer. Res. 2008; 14:1377–1385. [PubMed: 18316558] c) Jahn M, Radchenko V, Filosofov D, Hauser H, Eisenhut M, Rosch F, Jennewein M. Radiochim. Acta. 2010; 98:807–812.d) Herth MM, Barz M, Jahn M, Zentel R, Rosch F. Bioorg. Med. Chem. Lett. 2010; 20:5454–5458. [PubMed: 20709549]
6. a) Yavuz CT, Mayo JT, Yu WW, Prakash A, Falkner JC, Yean S, Cong L, Shipley HJ, Kan A, Tomson M, Natelson D, Colvin VL. Science. 2006; 314:964–967. [PubMed: 17095696] b) Yean S, Cong L, Yavuz CT, Mayo JT, Yu WW, Kan AT, Colvin VL, Tomson MB. J. Mater. Res. 2005; 20:3255–3264.c) Chandra V, Park J, Chun Y, Lee JW, Hwang IC, Kim KS. ACS Nano. 2010; 4:3979–3986. [PubMed: 20552997] d) Raven KP, Jain A, Loeppert RH. Environ. Sci. Technol. 1998; 32:344–349.
7. a) Morin G, Wang Y, Ona-Nguema G, Juillot F, Calas G, Menguy N, Aubry E, Bargar JR, Brown GE Jr. Langmuir. 2009; 25:9119–9128. [PubMed: 19601563] b) Wang Y, Morin G, Ona-Nguema G, Juillot F, Calas G, Brown GE Jr. Environ. Sci. Technol. 2011; 45:7258–7266. [PubMed: 21809819]
8. a) Chen F, Bu WB, Chen Y, Fan YC, He QJ, Zhu M, Liu XH, Zhou LP, Zhang SJ, Peng WJ, Shi JL. Chem. Asian. J. 2009; 4:1809–1816. [PubMed: 19902450] b) Park J, An K, Hwang Y, Park JG, Noh HJ, Kim JY, Park JH, Hwang NM, Hyeon T. Nat. Mater. 2004; 3:891–895. [PubMed: 15568032]
9. Zhang T, Ge J, Hu Y, Yin Y. Nano. Lett. 2007; 7:3203–3207. [PubMed: 17854231]
10. Shehata MM, Scholten B, Spahn I, Coenen HH, Qaim SM. J. Radioanal. Nucl. Chem. 2011; 287:435–442.
11. a) Shi R, Jia Y, Wang C. J. Environ. Sci. 2009; 21:106–112.b) Violante A, Pigna M. Soil Sci. Soc. Am. J. 2002; 66:1788–1796.
12. Choi HS, Liu W, Misra P, Tanaka E, Zimmer JP, Ipe B. Itty, Bawendi MG, Frangioni JV. Nat Biotechnol. 2007; 25:1165–1170. [PubMed: 17891134]
13. Glaus C, Rossin R, Welch MJ, Bao G. Bioconjug. Chem. 2010; 21:715–722. [PubMed: 20353170]
14. Luciani A, Itti E, Rahmouni A, Meignan M, Clement O. Eur. J. Radiol. 2006; 58:338–344. [PubMed: 16473489]
15. a) Mehlen P, Puisieux A. Nat. Rev. Cancer. 2006; 6:449–458. [PubMed: 16723991] b) Nguyen DX, Bos PD, Massague J. Nat. Rev. Cancer. 2009; 9:274–284. [PubMed: 19308067]
16. a) Hong H, Yang K, Zhang Y, Engle JW, Feng L, Yang Y, Nayak TR, Goel S, Bean J, Theuer CP, Barnhart TE, Liu Z, Cai W. ACS Nano. 2012; 6:2361–2370. [PubMed: 22339280] b) Hong H, Yang Y, Zhang Y, Engle JW, Barnhart TE, Nickles RJ, Leigh BR, Cai W. Eur. J. Nucl. Med. Mol. Imaging. 2011; 38:1335–1343. [PubMed: 21373764] c) Cai W, Shin DW, Chen K, Gheysens O, Cao Q, Wang SX, Gambhir SS, Chen X. Nano. Lett. 2006; 6:669–676. [PubMed: 16608262] d) Cai W, Chen K, Mohamedali KA, Cao Q, Gambhir SS, Rosenblum MG, Chen X. J. Nucl. Med. 2006; 47:2048–2056. [PubMed: 17138749] e) Nolting DD, Nickels ML, Guo N, Pham W. Am. J. Nucl. Med. Mol. Imaging. 2012; 2:273–306. [PubMed: 22943038]
17. a) Xie J, Chen K, Huang J, Lee S, Wang J, Gao J, Li X, Chen X. Biomaterials. 2010; 31:3016–3022. [PubMed: 20092887] b) Park JC, Yu MK, An GI, Park SI, Oh J, Kim HJ, Kim JH, Wang EK, Hong IH, Ha YS, Choi TH, Jeong KS, Chang Y, Welch MJ, Jon S, Yoo J. Small. 2010; 6:2863–2868. [PubMed: 21104828] c) Martin de Rosales, R. Torres; Tavare, R.; Paul, RL.; Jauregui-Osoro, M.; Protti, A.; Glaria, A.; Varma, G.; Szanda, I.; Blower, PJ. Angew. Chem. Int. Ed. 2011; 50:5509–5513.d) Sandiford L, Phinikaridou A, Protti A, Meszaros LK, Cui X, Yan Y, Frodsham G, Williamson PA, Gaddum N, Botnar RM, Blower PJ, Green MA, de Rosales RT. ACS Nano. 2013; 7:500–512. [PubMed: 23194247]

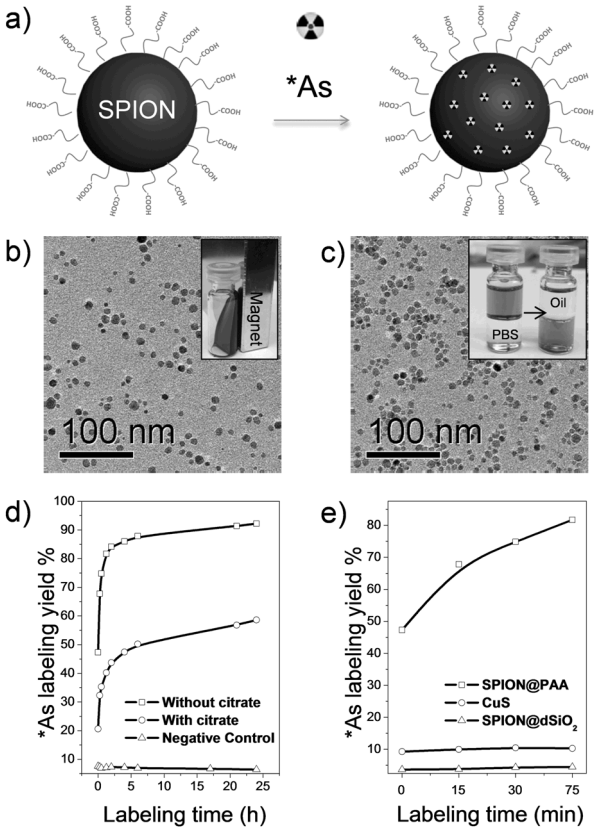

Figure 1.

(a) Schematic illustration of chelator-free synthesis of *As-SPION. (b) TEM image of SPION@OA. Inset is a photo showing the ferrofluidic behavior of SPION@OA in cyclohexane at room temperature. (c) TEM image of SPION@PAA. Inset shows the transfer of SPION@OA from the oil phase (cyclohexane) to aqueous phase (PBS, pH 7.4) via the PAA for OA ligand exchange process. (d) Time-dependent *As-labeling yield of SPION@PAA and partial absorption blocking with the presence of sodium citrate competitive ions. Negative control group has only water (pH 7-8, 1 mM of sodium hydroxide) and radioarsenic (~6 MBq). (e) Influence of nanoparticle surface on *As-labeling yield.

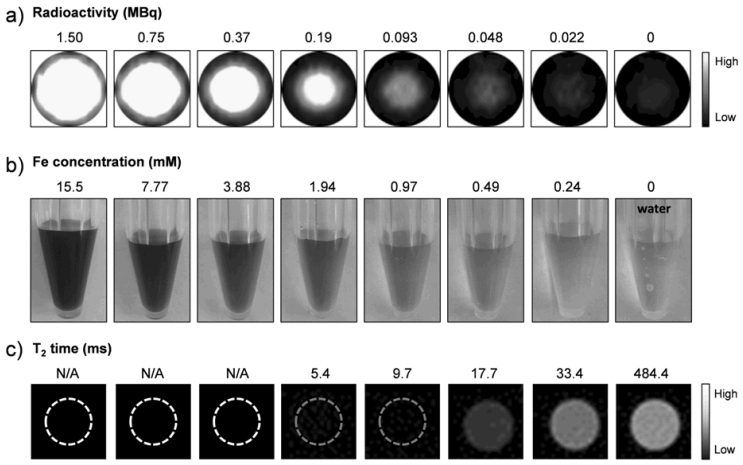

Figure 2.

(a) PET imaging of *As-SPION (in 0.25 mM HEPES buffer) with varied radioactivity level (from 0 to 1.50 MBq). (b) Digital photos and (c) corresponding T_2*-weighted MR images of SPION@PAA with varied Fe concentrations from 0 to 15.5 mM. T_2 relaxation time was too short to be measured at Fe concentrations equal to or exceeding 3.88 mM (indicated by dashed circles).

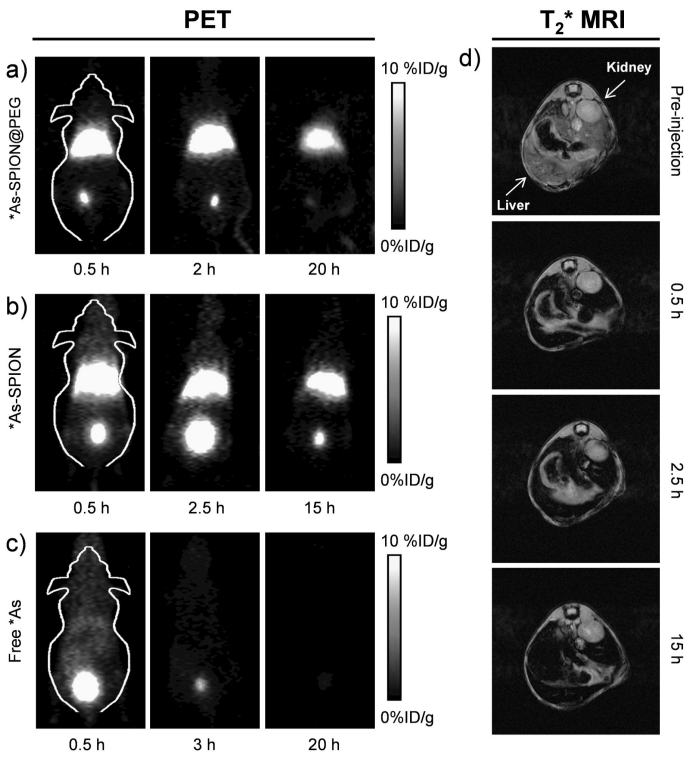

Figure 3.

Serial in vivo PET images of (a) PEGylated *As-SPION, (b) non-PEGylated *As-SPION and (c) free *As at different time points after intravenous injection into mice. (d) In vivo T_2*-weighted MR images of mice before and after intravenous injection of SPION@PAA (in PBS). Transaxial images were presented to show the liver uptake of SPION@PAA.

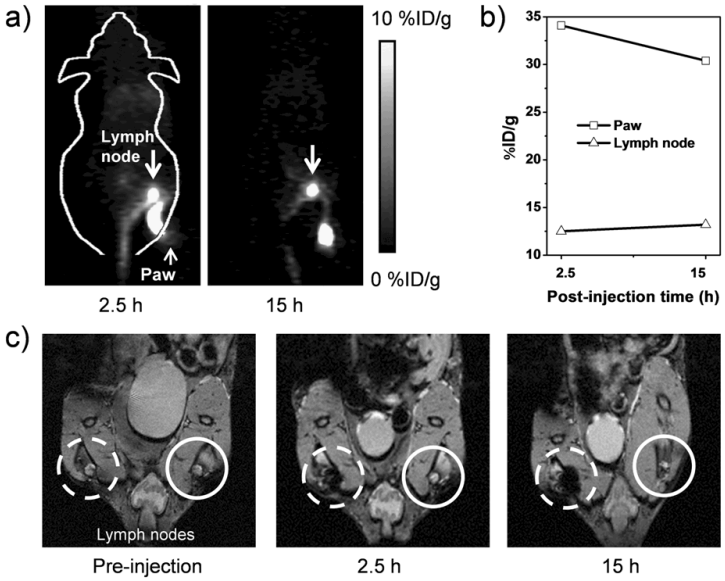

Figure 4.

(a) In vivo lymph node imaging with PET, after subcutaneous injection of *As-SPION@PEG into the right footpad of mouse. (b) Quantification of *As-SPION@PEG uptake in the lymph node and mouse paw. (c) In vivo lymph node mapping with MRI before and after injection of SPION@PAA to the left footpad of mouse. Obvious darkening of the lymph node could be seen (dashed circle) where the contralateral lymph node (solid circle) showed no contrast enhancement.